Check for updates

Anionic ribose related species explored through PES experiments, DFT calculations, and through comparison with anionic fructose species†

Zhen Zeng and Elliot R. Bernstein (ID) *

Ribose related species, (ribose-H)⁻ and (ribose-H₂O)⁻, are investigated through anion photoelectron spectroscopy (PES) combined with density functional theory (DFT) calculations. Their vertical detachment energies (VDEs) are experimentally determined and their anionic structures with positional and conformational isomers are definitively assigned. The ribose⁻ parent anion is not detected in the present experiments. (ribose-H)⁻ and (ribose-H₂O)⁻ anions can be accessed as the characteristic fragmentation ions of the parent species. Generation of (ribose-H)⁻ through the matrix assisted laser desorption ionization (MALDI) process is sample desorption substrate dependent, while generation of (ribose-H₂O)⁻ is independent of a wide range of desorption substrates. Both conformational and positional isomers of (ribose-H)⁻ are identified in the gas phase. Two types of positional isomers of (ribose-H₂O)⁻ (both from open chain structures) are assigned to contribute to two different components of the observed PES feature. The dehydration process can be thermodynamically accessed through both the parent anion and the neutral. A comparison between the PES and DFT results of ribose and fructose leads to the general conclusions: (1) ribose⁻ open chain structures are more likely to lose hydrogen from C atoms than fructose⁻ open chain structures, especially from (2)C and (4)C positions; (2) ribofuranose⁻ has a relatively higher propensity for loss of H than does fructofuranose⁻ in our MALDI/ablation process; and (3) the ribofuranose⁻ anion has lower decomposition probability through loss of water compared to the fructofuranose⁻ anion.
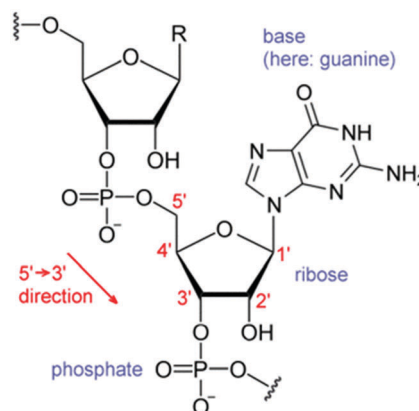
I. Introduction

Ribose, constituting a subunit of the RNA (ribonucleic acid) backbone, is an essentially important monosaccharide: ribose also appears as a substrate in ATP/ADP/AMP (adenosine tri/di/mono-phosphate). As both a building block for RNA and an energy carrier for ATP..., ribose plays key roles in structural and functional biology, nutrition, and human health. Conformational behavior and fragmentation mechanism studies of monosaccharides continue to be fields of great research interest, as monosaccharides in general are critical for understanding structural and functional implications for biochemical building blocks, biological catalysis, and molecular recognition.

Monosaccharides are flexible polymorphic species, presenting rich and complex constitutional, configurational, and conformational isomerism. In solution, ribose exists as an equilibrium mixture of α- and β-pyranose and α- and β-furanose structures; the dominant

solution structure, however, is β-pyranose.[1–4] The crystal structure for solid phase ribose exhibits α- and β-pyranose configurations in various ratios.[5] The biologically relevant structure of ribose is the ribofuranose form, such as in RNA, as seen in Scheme 1. Condensed phase studies of ribose underscore the environmental and conditional effects on its conformational preferences.

Scheme 1 Structures of RNA (from wikipedia).

Department of Chemistry, NSF ERC for Extreme Ultraviolet Science and Technology, Colorado State University, Fort Collins, CO 80523, USA. E-mail: erb@colostate.edu

† Electronic supplementary information (ESI) available: More low lying isomers of ribose⁻, (ribose-H)⁻, and (ribose-H₂O)⁻ as well as their corresponding neutrals. See DOI: 10.1039/c7cp05830f
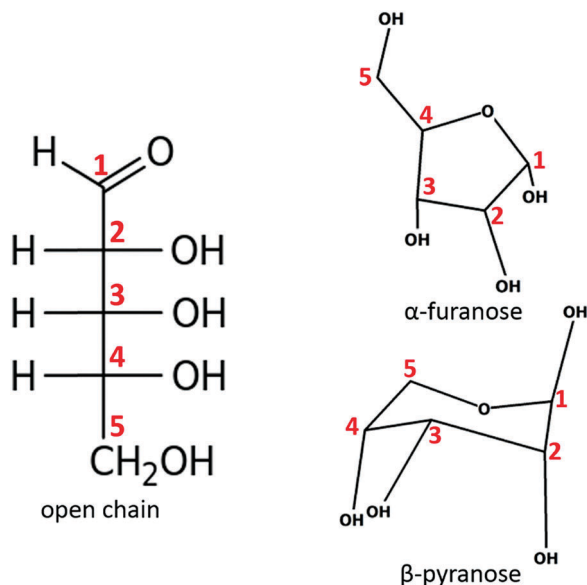
Fig. 1 Schematic structures of D-ribose with C atom numbering.

Gas phase, isolated ribose investigation can reveal intrinsic conformational information. Microwave spectroscopy, in conjunction with supersonic jet expansion and ultrafast UV laser vaporization, demonstrates that free neutral ribose (see Fig. 1) preferentially adopts a β-pyranose lower energy structure. In addition, higher energy α-pyranose forms can also be identified.[6] No evidence of α-/β-furanoses or linear forms is found for gas phase ribose using microwave techniques. Biological systems display β-furanoses as reported for RNA and ATP….

A full theoretical exploration of the conformational landscape for isolated D-ribose in terms of open chain, pyranose, and furanose conformations has been performed at two DFT (B3LYP and M06-2X) computational levels by considering over a thousand initial structures. This study suggests that α- and β-pyranose structures are the most populated according to both functionals.[7] Another computational study also probes conformations of gas phase ribose and generates populated structural results that are consistent with the experimental microwave determination.[8]

Experimental investigations of ionized ribose are rare, but nevertheless important as they can help understand ribose stability, fragmentation mechanisms, as well as radiation damage mechanisms in cellular systems. Gas phase studies of deprotonated ribose provide fragmentation patterns and identify two types of cross-ring cleavage mechanisms,[9] but conformational information of the fragmentation is not readily accessible.

Studies of conformation, as well as fragmentation mechanisms, for anionic ribose provide a pathway to elucidation of secondary low energy electron radiation damage mechanisms for DNA, RNA, and other species in cellular systems. Low energy electrons can induce single- and/or double-strand breaks in DNA.[10,11] Low energy electron damage studies for both condensed phase DNA and gas phase isolated DNA molecules suggest that electron resonances (*i.e.*, the formation of transient anions) play a dominant role in the fragmentation associated with electron energy <15 eV.[12] From the experimental DEA (dissociative

electron attachment) investigation of thymidine (thymine joined to sugar), the sugar moiety can capture low energy (0–3 eV) electrons, leading to subsequent fragmentation at the rupture of the N1–C1 bond between the thymine and sugar moieties.[13] Detailed DEA experiments on D-ribose are also performed: they reveal that very low energy electrons (0–1 eV) induce decomposition reactions associated with the loss of neutral water molecules and carbon containing neutral moieties leading to degradation of ring structures.[14] Isotopic labeling enables the sites involved in the fragmentation reaction to be identified. In this study, ribose is assumed to exist in a pyranose form. Full conformational anionic structures need to be explored in order to obtain a more comprehensive understanding of the dissociation pathway mechanisms. Another electron attachment experiment for ribose in the energy range ∼8 eV, coupled with resonance dynamic calculations (furanosic and pyranosic structures), reveals the formation of transient negative ions and suggests possible ring breaking pathways.[15] The quantum chemical theoretical investigation of anionic ribose has been conducted to understand the mechanism of DEA at an atomic/molecular level. The study concludes that observed DEA fragmentation processes arise from electron attachment to open chain, but not cyclic, conformations.[16]

Unveiling monosaccharide conformation, stability, and activity provides important insights and clues to the exclusively evolved ribose as a component in nucleic acids, *etc.* based on prebiotic chemistry. The ribonucleotides have nine required chemoselectivities:[17] (1) aldose not ketose; (2) pentose not tetrose, hexose, *etc.*; (3) ribo, not arabino, lyxo, or xylo; (4) furanosyl not pyranosyl; (5) β not α; (6) D not L; (7) regiospecifically glycosylated; (8) regiospecifically phosphorylated; and (9) activation toward regiospecific oligomerization. By comparing the sugar pucker conformations and configurations of pentose, β-D-ribose fits best into the structure of physiological forms of nucleic acids.[18] A theoretical mechanism has additionally been proposed from the point of view of enantiomeric purity of ribose.[19] Ribose is reportedly the easiest racemic monosaccharide to separate into enantiomers, which can also contribute to an explanation for the evolutionary selection of ribose above other saccharide species for its biological importance.

Activation of ribose for nucleoside formation has also been explored through[20] investigation of the reaction between sugar and cyanamide ($NCNH_2$), as well as the further crystallization of the sugar-cyanamide from aqueous solution. Additionally, ribose undergoes preferential sequestration due to its greater reactivity with respect to other sugars and through formation of chirally pure crystal domains even from racemic starting materials.

Some systematic experimental studies have been undertaken to synthesize potential alternatives identical to the nucleic acid structure, and compare them with natural nucleic acids with respect to their functional biochemical properties. The report considers the synthetic system's capacity for informational base paring in the Watson–Crick mode. It concludes that three hexoses (hexopyranosyl oligonucleotides mimicking the RNA/ribose connections) could not have acted as viable competitors to natural RNA/ribose species because of their steric bulk.[21]

This journal is © the Owner Societies 2017

Phys. Chem. Chem. Phys., 2017, **19**, 28950–28962 | **28951**

Investigation of the conformations of ribose related anionic species may help to understand fragmentation mechanisms, as well as the stability and activity of ribose with regard to its natural selection for biopolymer backbone supports. In the present paper, the issue concerning RNA/DNA sugar moiety selection will be discussed from the point of view of electronic states of observed anion and neutral species, in addition to the above saccharide structural and steric properties and stabilities. Anion stability and fragmentation behavior can also contribute to the overall stability of these essential genetic code features.

In the present work, we conduct PES experiments and DFT calculations on gas phase, isolated ribose related anionic species in order to investigate their electronic and geometric structures. The isolated ribose parent anion and related species are explored, and both their electronic and geometric structures are revealed through comparison of experimental and calculated VDEs. The anionic structures (conformational and positional) of (ribose-H)$^-$ and (ribose-H$_2$O)$^-$ that exist in the present experiments are assigned based on the agreement between calculated and observed VDEs. Conformational isomers (open chain, furanose, pyranose, ...) have different geometries, but the same positions for loss of one H atom, a H atom and an OH group, or a H$_2$O moiety. Positional isomers have different fragmented moiety positions, but with similar conformations. Parent ribose$^-$ and (ribose-OH)$^-$ anions are not detected. The related fragment species (ribose-H)$^-$ is dependent on the MALDI sample desorption substrates, while the (ribose-H$_2$O)$^-$ species present in the experimental sample are independent of desorption substrates. Formation mechanisms for (ribose-H)$^-$ and (ribose-H$_2$O)$^-$ are calculated and identified. A comparison between the ribose results and the fructose results[22] is also presented.

II. Experimental procedures

The experimental apparatus consists of three parts: a pulsed supersonic nozzle with an attached matrix assisted laser desorption ionization (MALDI) source, a reflectron time of flight mass spectrometer (RTOFMS), and a magnetic bottle photoelectron TOF spectrometer (MBTOFPES). Details of this system (RTOFMS/MBTOFPES) can be found in our previous publications.[23,24] The nozzle employed for the sample beam generation is constructed from a Jordan Co. pulsed valve and a laser desorption attachment. All sample drums for the MALDI are prepared by wrapping different sample desorption substrates (Zn, Al or Cu) on a clean Al drum.[25] A mixed solution of D-ribose and the matrix (R6G or DCM) dye with a mole ratio of ~3:2 in a solvent (typically, methanol or acetonitrile) is uniformly sprayed on the drum/substrate surface using an air atomizing spray nozzle (Spraying System Co.) with a siphon pressure of 10 psi. During the spraying process, the sample drum is rotated under heat of a halogen lamp in a fume hood to ensure deposition of D-ribose and the matrix on the drum surface is homogeneous and dry. The well coated and dried sample drum is then placed in the laser ablation head/ nozzle assembly and put into the vacuum chamber. Second

harmonic (532 nm) light pulses from a Nd:YAG laser are used to ablate the sample drum, which rotates and translates simultaneously to maintain a fresh sample area for each laser ablation pulse. Whole D-ribose molecules desorbed from the drum, interacting with other species (including electrons) in the ablated material plume, are entrained in the supersonic flow of helium carrier gas with a 50 psi backing pressure through a 2 × 60 mm channel in the ablation head, and expanded into the sample chamber. With a closed pulsed valve, the RTOFMS chamber pressure is ~6 × 10^{-8} Torr. Generated molecular anions are pulsed into the RTOFMS and are mass analyzed using the RTOFMS. For PES experiments, specific anions are first mass selected and decelerated before interacting with a 355 nm (3.496 eV), or 266 nm (4.661 eV) laser beam from another Nd:YAG laser in the photodetachment region. Photo-detached electrons are collected and energy analyzed by the MBTOFPES at nearly 100% efficiency. The photodetachment laser is operated at a 10 Hz repetition rate, while the ablation laser is synchronously triggered at 5 Hz. Data are collected at 5 Hz employing a background subtraction with alternation of the ablation laser on/off if the detachment laser generates 266 nm or higher energy photons. Every photoelectron spectrum is calibrated by the known spectra of Cu$^-$ at the employed detachment photon energy. The photoelectron energy resolution is ~4% (40 meV for 1 eV kinetic energy electrons), as anticipated for a 1 m PES flight tube.

III. Computational methods

DFT (B3LYP and M062X functionals) methods with a 6-311++G(d,p) basis set were validated to be efficient and accurate for electronic and geometric property calculations of gas phase sugar molecular anions and neutrals based on fructose recently reported studies.[22] The calculational approach has also been justified in a previous paper.[22] Briefly, for the computationally large sugar molecule and molecular anion, ribose C$_5$(H$_2$O)$_5$, one must explore the various available computational algorithms to determine which approximate method will best predict the experimental results efficiently, reproducibly, and reliably. The present theoretical studies are evaluated and justified for ribose related molecular anions through the best agreement for VDEs between predictions and observations. By considering the preceding literature summarized in our previous paper[22] and our own experience with CASSCF, CASMP2, DFT, and MP2 calculations for energetic molecules, as well as DFT functionals (B3LYP and M062X) for fructose, B3LYP/6-311++G(d,p) and M062X/6-311++G(d,p) levels of theories are chosen for current calculations. In the present work, all calculations are executed using density function theory (DFT) employing Becke's three-parameter hybrid (B3LYP)[26–28] functional and a 6-311++G(d,p) basis set for all atoms, as implemented in the Gaussian 09 program.[29] The low energy isomers for every species are reoptimized employing a M062X[30,31] functional with the same basis set. The ωB97XD[32] functional and the MP2 method are also chosen for additional comparison of several typical (ribose-H$_2$O)$^-$ isomers

calculated using different functionals and methods. No symmetry restrictions are applied for the calculations. Optimization of the low lying isomers for each anion and neutral are performed with harmonic vibrational frequencies calculated to confirm that the obtained structures are the true local minima. Theoretical VDEs for each anionic species are calculated as the energy difference between the ground state of the anion and its corresponding neutral at the same structure as the anion. For further electronic structure based understanding of the observed ribose related species behavior, a Natural Bond Orbital (NBO) analysis is performed based on the B3LYP functional and the 6-311++G(d,p) basis set.

IV. Experimental results

Through MALDI processes, (ribose-H)$^-$ and (ribose-H$_2$O)$^-$ can be generated and detected by spraying a sample on different substrates, but ribose$^-$ is not populated at high enough concentrations to be observed in the present experiments. Their photoelectron spectra are displayed in Fig. 2 and 3, respectively. VDEs are measured from the maxima of the corresponding PES peaks. The photoelectron spectrum of (ribose-H)$^-$, recorded using 266 nm photons and on different substrates, is shown in Fig. 2. It shows all broad features on three of the substrates, but with different feature shapes, especially at the low electron binding energy (EBE) portion ($< \sim 3$ eV) of the spectral feature. The peaks obtained on both Al and Cu have major components ranging from ~ 3 eV to ~ 4.24 eV, but have a significantly higher intensity in the low EBE part of the feature centered at 1.96 eV with a Cu substrate. The PES feature generated with a Zn substrate mainly exhibits two features centered at ~ 3.27 and ~ 2.45 eV, respectively. These broad features are contributed by different isomers.

Fig. 3 Photoelectron spectrum of (ribose-H$_2$O)$^-$ recorded with 355 nm photons with sample (D-ribose/DCM) spayed on a Zn substrate.

The photoelectron spectrum of (ribose-H$_2$O)$^-$ recorded using 355 nm photons with the sample sprayed on a Zn substrate is displayed in Fig. 3. It mainly shows two slightly distinguishable components centered at ~ 1.53 and ~ 1.98 eV, as well as a long tail to above 3 eV. A similar PES feature can be obtained, as shown in Fig. S20 (ESI†), employing an Al substrate. The experimental VDEs of (ribose-H)$^-$ and (ribose-H$_2$O)$^-$ are summarized in Table 1.

V. Theoretical results

The low lying isomers of ribose related species are first optimized at the B3LYP/6-311++G(d,p) level of theory. The lower lying isomers of ribose$^-$, (ribose-H)$^-$, and (ribose-H$_2$O)$^-$ are then reoptimized via the M062X/6-311++G(d,p) approach based on the initial B3LYP structures. From these two approaches, we can obtain similar calculated VDEs of every specific isomer for each species, as shown in Table 1, and nearly identical geometrical structures, as can be seen in Fig. 4–6 and Fig. S16–S18 (ESI†). For ribose$^-$, the two levels of theory give rise to the same energy order of low lying isomers. For (ribose-H)$^-$, the calculated VDEs of isomers consistent with experiments can be obtained from both approaches but with slightly different energy order. For (ribose-H$_2$O)$^-$, as shown in Table 1 and Fig. 6 and Fig. S18 (ESI†), both functionals reveal similar lower energy isomers assigned to contribute to the experimental results, but with slightly different energy order. The first six lowest energy isomers of (ribose-H$_2$O)$^-$ are also reoptimized and their VDEs are calculated based on ωB97xd/6-311++G(d,p), and MP2/6-311++G(d,p). As shown in Table S1 (ESI†), the calculated VDEs employing a ωB97xd functional are indistinguishable from those generated by the other two functionals. The VDEs calculated at the MP2 level are smaller by ~ 0.5 eV than the experimental ones.
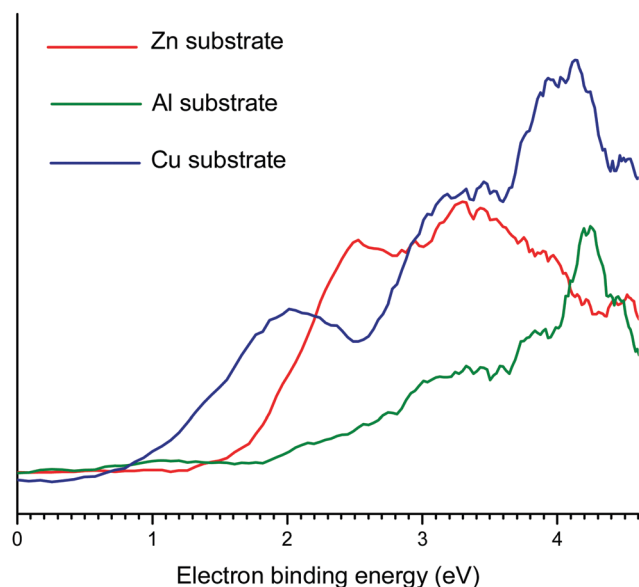

Fig. 2 Photoelectron spectrum of (ribose-H)$^-$ recorded with 266 nm photons with sample (D-ribose/DCM or R6G) spayed on different absorption substrates.
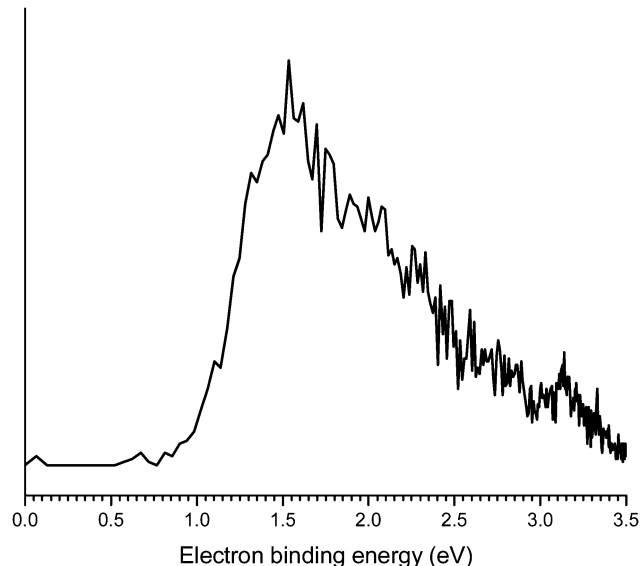
This journal is © the Owner Societies 2017

Phys. Chem. Chem. Phys., 2017, 19, 28950–28962 | 28953

Table 1 Relative energies (ΔE) of the low energy isomers of ribose⁻, (ribose-H)⁻, and (ribose-H₂O)⁻, and comparison of their calculated VDEs based on B3LYP/6-311++G(d,p) and M062X/6-311++G(d,p) algorithms. Experimental VDE values are given in the right hand column. All energies are in eV

		B3LYP/6-311++G(d,p)		M062X/6-311++G(d,p)		
		ΔE	Theo. VDE	ΔE	Theo. VDE	Exp. VDE
ribose⁻	ribose⁻ (A)	0.00	1.64	0.00	1.48	—
	ribose⁻ (B)	0.01	1.73	0.01	1.57	
	ribose⁻ (C)	0.17	1.51	0.19	1.37	
	ribose⁻ (D)	0.25	1.06	0.29	0.92	
	ribose⁻ (E)	0.80	−0.25	0.64	−0.52	
	ribose⁻ (F)	0.81	−0.17	0.66	−0.45	
	ribose⁻ (G)	0.81	−0.03	0.78	−0.34	
	ribose⁻ (H)	0.87	−0.03	0.79	−0.21	
(ribose-H)⁻	(ribose-H)⁻ (A)	0.00	3.16	0.38	3.51	∼3.27 to ∼4.24
	(ribose-H)⁻ (B)	0.11	4.47	0.19	4.63	
	(ribose-H)⁻ (C)	0.22	3.75	0.00	3.87	
	(ribose-H)⁻ (D)	0.25	3.91	0.30	4.17	
	(ribose-H)⁻ (E)	0.27	2.74	0.37	2.73	∼2.45
	(ribose-H)⁻ (F)	0.27	3.79	0.14	3.86	
	(ribose-H)⁻ (G)	0.27	3.83	0.00	4.16	
	(ribose-H)⁻ (H)	0.28	2.64	0.37	2.65	
	(ribose-H)⁻ (I)	0.29	3.93	0.34	4.11	
	(ribose-H)⁻ (J)	0.35	3.72	0.17	3.75	
	(ribose-H)⁻ (K)	0.42	2.99	0.36	3.53	
	(ribose-H)⁻ (L)	0.45	2.54	0.54	2.55	
	(ribose-H)⁻ (M)	0.52	3.32	0.29	3.48	
	(ribose-H)⁻ (N)	0.86	2.25	0.94	2.25	
(ribose-H₂O)⁻	(ribose-H₂O)⁻ (A)	0.00	3.13	0.03	3.17	
	(ribose-H₂O)⁻ (B)	0.04	3.09	0.00	3.03	
	(ribose-H₂O)⁻ (C)	0.32	2.16	0.26	2.13	∼1.98
	(ribose-H₂O)⁻ (D)	0.41	1.50	0.13	1.41	∼1.53
	(ribose-H₂O)⁻ (E)	0.43	1.58	0.13	1.51	
	(ribose-H₂O)⁻ (F)	0.44	1.97	0.37	2.02	
	(ribose-H₂O)⁻ (G)	0.57	1.50	0.19	1.26	
	(ribose-H₂O)⁻ (H)	0.85	3.85	0.71	4.11	
	(ribose-H₂O)⁻ (I)	0.94	3.90	0.81	3.89	
	(ribose-H₂O)⁻ (J)	1.27	3.30	1.09	3.05	
	(ribose-H₂O)⁻ (K)	1.29	0.75	1.27	1.32	

The low lying isomers of ribose⁻, (ribose-H)⁻, and (ribose-H₂O)⁻ anions, as well as their corresponding neutrals, are summarized in Fig. 4–6 and Fig. S10–S12 (ESI†). More isomers are presented in the ESI.† Note that the figure numbers in the ESI† document are related to those of the text figures, as for example Fig. 4 ⇔ Fig. S4 (ESI†). Calculated VDEs and relative energies of their anions are summarized and compared with the experimental results in Table 1. Although optimized neutral structures are not necessarily directly related to their respective experimental VDE results, the low lying isomers of neutrals are provided to show their structural characteristics and for comparison with anions.

Typical low lying isomers of the ribose⁻ anion are shown in Fig. 4. Both DFT functionals B3LYP and M062X find open chain structures to be the lowest energy isomers with positive calculated VDEs above 1 eV. The cyclic structures are higher in energy than the most stable open chain structure by ∼0.8 eV from the B3LYP functional and ∼0.7 eV from the M062X functional; however, they show negative calculated VDEs. Their neutral counterparts are exhibited in Fig. S10 (ESI†) with the B3LYP/6-311++G(d,p) level of theory, which displays a pyranose structure (ribose (a)) as the most stable neutral ribose. Its electron affinity (EA) is calculated to be −0.21 eV.

For geometrical optimization of (ribose-H)⁻, all lower lying isomers of ribose⁻ are chosen to be the initial structures followed by loss of a H atom at different possible positions. The subsequent low lying isomers of (ribose-H)⁻ are presented in Fig. 5. More isomers are shown in Fig. S5 (ESI†). Isomer (ribose-H)⁻ (A) is derived from parent open chain ribose⁻ (C) by losing H from the C atom at the (4) position (labeled as (4C)H). It undergoes (2)C–(3)C bond breaking and intramolecular hydrogen bond formation. Its theoretical VDE is calculated to be 3.16 eV, in the range of the broad experimental PES feature. Isomer (ribose-H)⁻ (B) is developed from parent open chain ribose⁻ (C) through loss of H from the O atom on the (3) position (labeled as (3)H). It has a calculated VDE of 4.47 eV, in good agreement with the experimentally determined one. Isomer (ribose-H)⁻ (C) has geometry evolved from a pyranose structure with loss of (2)H and has a theoretical VDE of 3.75 eV, consistent with experiments. (ribose-H)⁻ (D) and (ribose-H)⁻ (I) develop from parent open chain ribose⁻ (A) and (B), respectively, both losing (2)H. Their calculated VDEs are 3.91 and 3.93 eV, respectively, in good agreement with the broad PES features. Isomer (ribose-H)⁻ (E) loses (2C)H from parent open chain ribose⁻ (B). It has a calculated VDE of 2.74 eV, in reasonable accord with the low EBE area of the 2.45 eV PES feature.
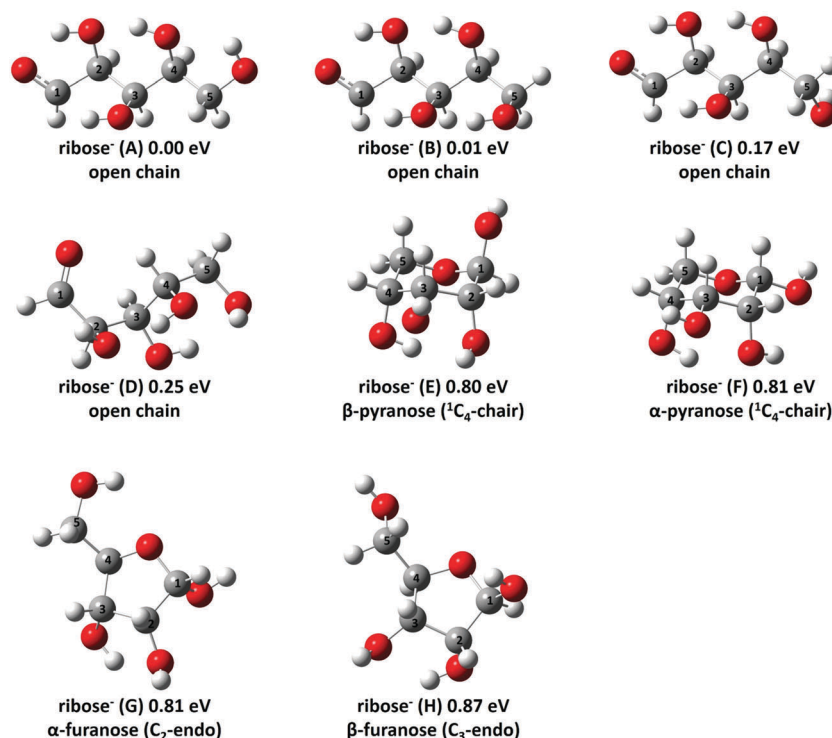
Fig. 4 Optimized geometries of typical low lying anionic isomers of ribose⁻ based on B3LYP/6-311++G(d,p) calculations. The relative energies and structural polymorphs are indicated. The C atom numberings are given. For open chain structures (1)C to (5)C is ordered from left to right. For both furanose and pyranose structures (1)C to (5)C is ordered from right to left in a clockwise direction. C atom numbering for open chain structures corresponds to that in cyclic structures; for instance, (1)C ⇔ (1)C.

Similarly, isomers (ribose-H)⁻ (H) and (ribose-H)⁻ (L) also lose (2C)H from open chain structures and have lower calculated VDEs (2.64 and 2.54 eV, respectively), in good agreement with the experimental one (2.45 eV) at the low EBE part of the PES feature. Isomer (ribose-H)⁻ (N) can evolve from parent open chain ribose⁻ (D) also by losing (2C)H, and displays a relatively high energy for a (ribose-H)⁻ species. Its calculated VDE is 2.25 eV, close to the low EBE feature (1.96 eV) in the spectrum of (ribose-H)⁻ employing a Cu substrate. Isomers (ribose-H)⁻ (F) and (ribose-H)⁻ (G) have furanose structures with dissociated (1)H and (3)H, respectively. Their theoretical VDEs are 3.79 and 3.83 eV, and are in accord with high EBE parts of the spectrum. There are more isomers with loss of H from an O atom at different positions evidencing reasonable VDEs compared to the high EBE ones from experiments, but they also possess dramatically higher energies than the most stable isomer. Thus, the high EBE components of the broad feature in the photoelectron spectrum of (ribose-H)⁻ are mainly contributed by open chain, pyranose, and furanose structures with loss of H from an O atom at different positions, as well as a few open chain isomers with loss of H from the (4)C atom. They are isomeric with both positional and conformational characteristics. The low EBE areas of the PES feature are mostly contributed by open chain isomers with loss of H from the (2)C atom ((2C)H).

The typical low lying anionic isomers of (ribose-H₂O)⁻ are displayed in Fig. 6: the green squares on the structures indicate loss of hydrogen and the green circles indicate loss of an OH group at the indicated positions. Isomers (ribose-H₂O)⁻ (A) and (ribose-H₂O)⁻ (B) are both developed from open chain structures through loss of (2)H, loss of (4)OH, and with (2)C–(3)C bond breaking. One intramolecular hydrogen bond is formed in the former isomer and two such bonds are formed in the latter isomer. Their calculated VDEs are 3.13 and 3.09 eV, respectively, in the range of the high binding energy tail of the PES feature for (ribose-H₂O)⁻. Isomer (ribose-H₂O)⁻ (C) is also derived from the open chain structure by losing H from the (4C) position and OH from the (5) position. It also undergoes (2)C–(3)C bond breaking with two intramolecular hydrogen bonds of length 1.67 Å formed. The theoretical VDE of isomer (ribose-H₂O)⁻ (C) is calculated to be 2.16 eV, in good agreement with the higher EBE components (~1.98 eV) of the (ribose-H₂O)⁻ PES feature. Similarly, isomer (ribose-H₂O)⁻ (F) exhibits an open chain structure with the same positional character ((4C)H/(5)OH) as isomer (ribose-H₂O)⁻ (C) but with conformational difference. The isomer (F) VDE is also calculated to be 1.97 eV, in accord with the high EBE side of the experimental feature. Isomers (ribose-H₂O)⁻ (D) and (ribose-H₂O)⁻ (E) appear to be open chain structures both with loss of (2C)H and (3)OH, but with evident conformational differences. Their calculated VDEs are 1.50 and 1.58 eV, which are consistent with the lower EBE component (~1.53 eV) of the PES feature of (ribose-H₂O)⁻. Isomer (ribose-H₂O)⁻ (G) has a relative energy of 0.57 eV with regard to the lowest energy isomer and shows (2C)H/(3)OH loss positions. Its calculated VDE is 1.50 eV, consistent with experiments.
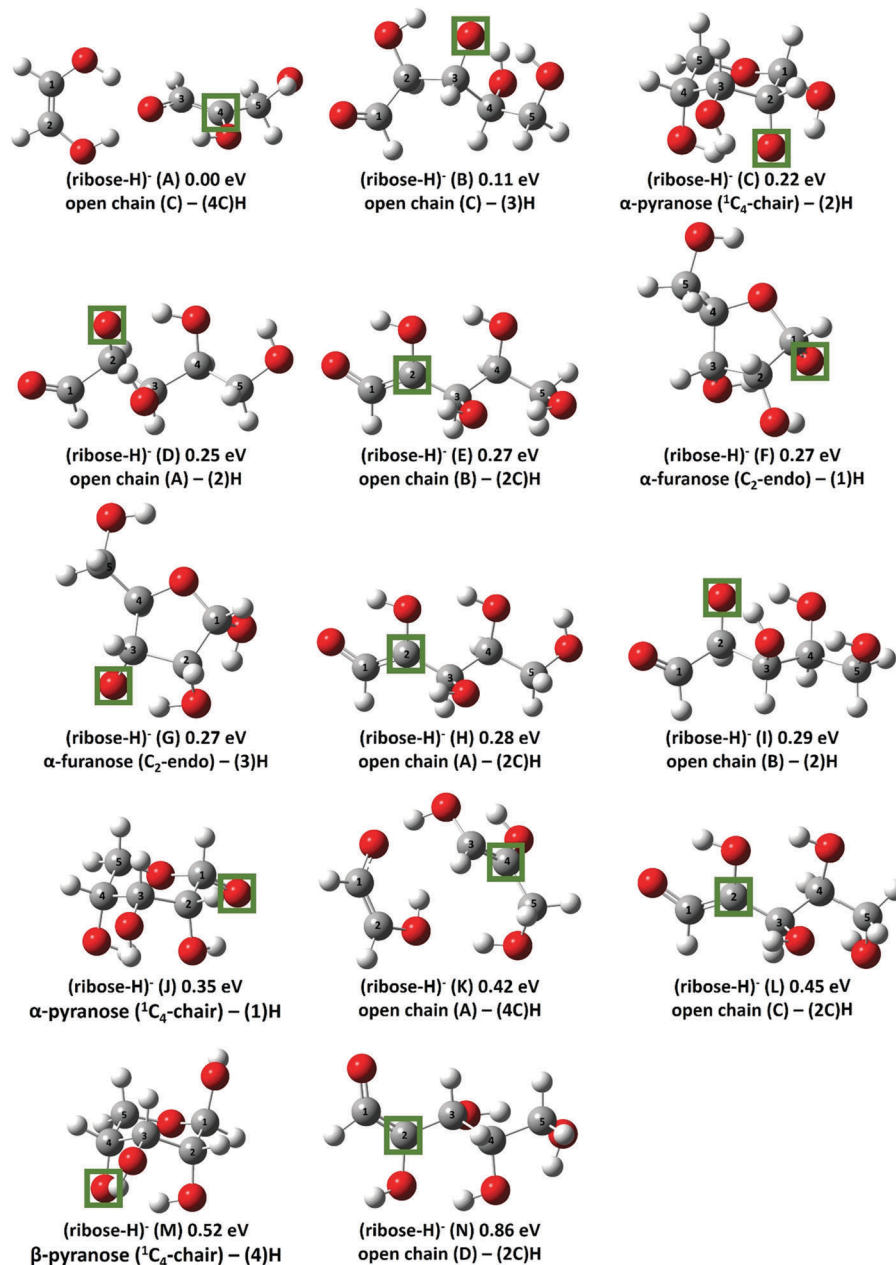
This journal is © the Owner Societies 2017

Phys. Chem. Chem. Phys., 2017, **19**, 28950–28962 | 28955

Fig. 5 Optimized geometries of typical low lying anionic isomers of (ribose-H)$^-$ based on B3LYP/6-311++G(d,p) calculations. The relative energies and structural polymorphs are indicated. The green square indicates loss of hydrogen at the indicated position. The C atom numberings are given. For open chain structures (1)C to (5)C is ordered from left to right. For both furanose and pyranose structures (1)C to (5)C is ordered from right to left in a clockwise direction. C atom numbering for open chain structures corresponds to that in cyclic structures; for instance, (1)C ⇔ (1)C.

Other isomers with higher relative energies have calculated VDEs out of the experimental feature width. Thus, the lower EBE components of the major peak in the spectrum of (ribose-H$_2$O)$^-$ are contributed by isomers (ribose-H$_2$O)$^-$ (D) and (E), and the higher EBE parts arise mainly from isomers (ribose-H$_2$O)$^-$ (C) and (F). Isomers (A) and (B) are less likely to be present to contribute the small tail of the peak. Isomer (G) may be present in our experiments too. The different PES feature components are generated by different positional isomers; the same PES feature components are composed of contributions from different conformational isomers.

VI. Discussion

A. Ribose related anionic species

1. Ribose$^-$. The ribose$^-$ parent anion is not populated in high enough concentration to be observed in the presented experiments. From our calculation results, the lowest energy isomers of the ribose$^-$ parent anion are the open chain ones. Pyranose and furanose anionic conformations have significantly higher relative energies and negative vertical detachment energies (~ −0.03 to −0.25 eV). Loss of one H atom or one
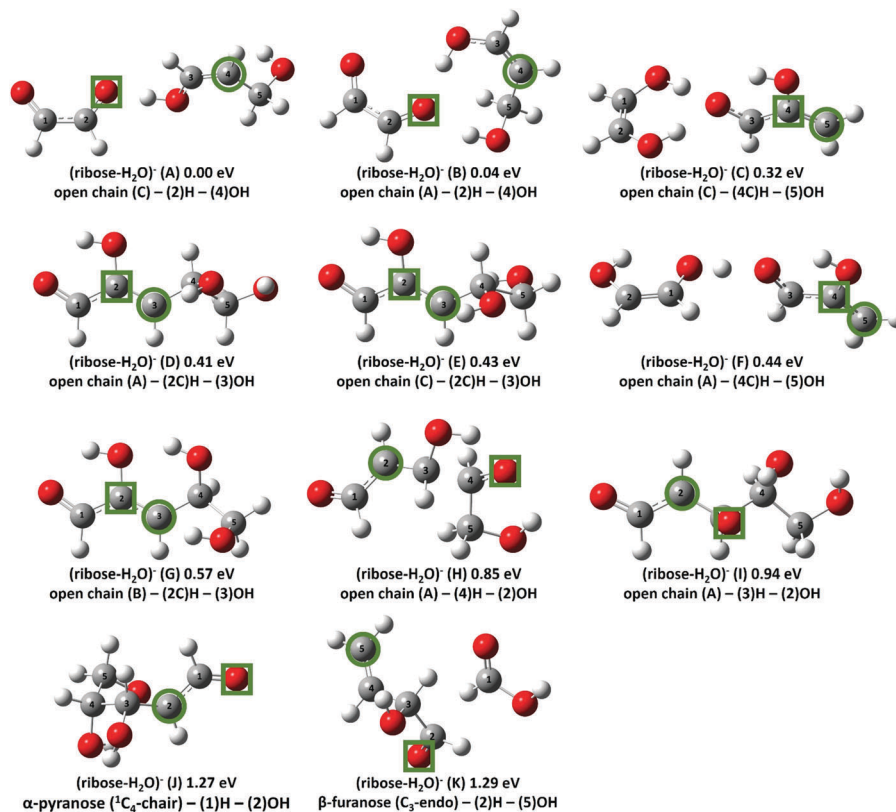
Fig. 6 Optimized geometries of the typical low lying anionic isomers of (ribose-H$_2$O)$^-$ based on B3LYP/6-311++G(d,p) calculations. The relative energies and structural polymorphs are indicated. The green square indicates loss of hydrogen and the green circle indicates loss of an OH group at the marked positions. The C atom numberings are given. For open chain structures (1)C to (5)C is ordered from left to right. For both furanose and pyranose structures (1)C to (5)C is ordered from right to left in a clockwise direction. C atom numbering for open chain structures corresponds to that in the cyclic structures; for instance, (1)C ⇔ (1)C.

H$_2$O moiety is characteristic of anionic fragmentation under the present experimental conditions. Based on the facts that the parent open chain ribose$^-$ anion should be generated in the MALDI/ablation process and that the isolated open chain ribose$^-$ anion has a lower energy than the isolated open chain ribose neutral, the parent anion of ribose must be unstable with respect to the (ribose-X)$^-$, X = H, H$_2$O species, and must therefore fragment in < 200 µs.

2. (Ribose-H)$^-$. The PES features of (ribose-H)$^-$ anions are substrate dependent and they appear to be in a broad electron binding energy range. Such a behavior suggests that many isomers with both positional and conformational characteristics coexist in the present experiments. The high EBE components (> ∼3 eV) are mostly contributed by isomers with loss of H from an O atom of open chain, pyranose, and furanose structures, with a few open chain isomers with loss of H from C atoms also present in the collection of these anion species. The low EBE components (< ∼3 eV) of the PES feature for this anion can be assigned to the higher energy open chain isomers with structures supporting loss of H from a (2)C atom.

3. (Ribose-H$_2$O)$^-$. (ribose-H$_2$O)$^-$ primarily exists as two kinds of positional isomers, one with loss of (4C)H and (5)OH, the other with loss of (2C)H and (3)OH, each contributing separately to the higher and lower EBE components of the broad PES feature. Both are only derived from open chain structures with loss of H from a C atom. Each positional isomer exhibits different conformations. Positional isomers (4C)H/(5)OH incur C–C bond breaking and form intramolecular hydrogen bonds, which help to stabilize and bind the resulting fragments.

B. Generation mechanisms

In a previous publication concerning reaction generation mechanisms for various fructose related anions,[22] we suggest possible reaction generation pathways for the observed species based on overall (equilibrium) thermodynamics for the process. Here we present enthalpy change ΔH values for different possible reaction pathways for generating specific ribose related anionic species. As shown in Fig. S19(a) (ESI†), ΔH for reactions from both anion and neutral parent ribose to generate (ribose-H)$^-$ isomers (A), (B), (C), and (E) are positive, implying that these reactions are thermodynamically forbidden (calculated entropy contributions are found to be small for the projected pathways). As shown in Fig. S19(b) (ESI†), the calculated ΔH for reactions from parent species to (ribose-H$_2$O)$^-$ following a step by step process is positive, while ΔH for a reaction through loss of one water molecule directly from parent anion/neutral species is negative. The results of these calculations suggest that the reaction pathway for generating (ribose-H$_2$O)$^-$ through direct

This journal is © the Owner Societies 2017

Phys. Chem. Chem. Phys., 2017, **19**, 28950–28962 | **28957**

loss of a H₂O molecule from parent anions/neutrals is thermodynamically allowed. Therefore, (ribose-H)⁻ is probably already present in the beam after the MALDI/ablation processes. (ribose-H₂O)⁻ can be generated either from the MALDI/ablation processes itself or from both reaction pathways from the parent anion or neutral through loss of one H₂O molecule directly. This conclusion is consistent with the experimental observation that the photoelectron spectrum of (ribose-H)⁻ is substrate dependent, and that similar PES features of (ribose-H₂O)⁻ are obtained with different substrates. Determination of fixed positions for loss of H₂O that are different from random loss of H from all C and O positions also suggests direct, spontaneous processes for loss of water.

C. Natural bond orbital (NBO) analysis of observed ribose related anionic species behavior

A Natural Bond Orbital (NBO) analysis is performed based on the B3LYP/6-311++G(d,p) level of theory to understand the observed ribose related anionic species behavior from the view point of the electronic structure. The molecular orbitals of
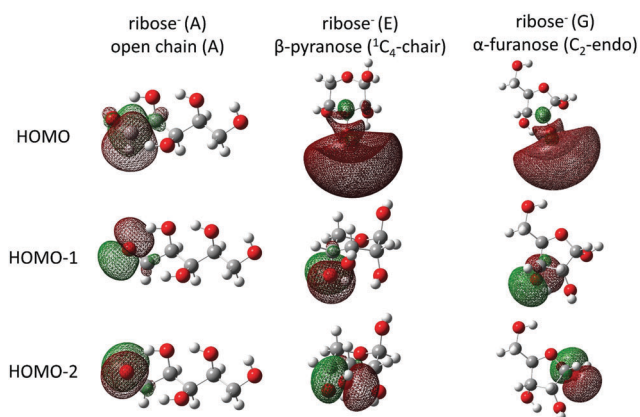

Fig. 7 Molecular orbitals of the lowest energy open chain, pyranose, and furanose structures of the ribose⁻ anion from an NBO analysis based on B3LYP/6-311++G(d,p) calculations.

specific isomers of ribose⁻, (ribose-H)⁻, and (ribose-H₂O)⁻, generated from an NBO analysis, are presented in Fig. 7–9.

As shown in Fig. 7, the HOMO (highest occupied molecular orbital) of the most stable open chain anion displays a valence bound anionic distribution mainly located in a p orbital of (1)C, while those of the most stable pyranose and furanose anions show diffuse dipole-bound states, for which the excess electron is mainly bound around the (3)H and (2)H atoms, respectively. The dramatic difference of electronic distributions further illustrates that open chain structures are more stable than cyclic structures for the ribose⁻ parent anion.

From Fig. 8, the HOMOs of three typical isomers (open chain, pyranose, and furanose) of (ribose-H)⁻ (B, C, and G) exhibit excess electron distribution in the p orbital of the O atom which undergoes loss of H. These isomers possess similar VDEs from different positional and conformational isomers. The HOMO of the isomer with loss of H from (2)C (E) displays an electron distribution localized on the (1)O atom.

Two positional isomers of (ribose-H₂O)⁻ evidence HOMO distributions mostly on the p orbital of the C atom from which the OH group is lost and its adjacent C atom from which the accompanying H atom is lost, as shown in Fig. 9. The site selective nature of the formation mechanism for these two positional isomers is not readily understandable based on the NBO analysis.

D. Comparison between the ribose and fructose results

Recall that for fructose TOFMS/PES experiments all (fructose-X)⁻, X = H, OH, H₂O and parent anions are observed, but for ribose, only (ribose-Y)⁻, Y = H, H₂O are detected in the TOFMS/PES data. We discuss these comparisons and contrasts below in detail.

a. Ribose⁻ and fructose⁻. Employing the same experimental apparatus and techniques, the ribose⁻ parent anion is not detected using PES, while the fructose⁻ parent anion is. The fructose⁻ parent anion exists in our experiments as open chain structures. The calculation results show that the lowest energy isomers of both ribose⁻ and fructose⁻ parent anions are open chain structures with the additional electron valence bound.
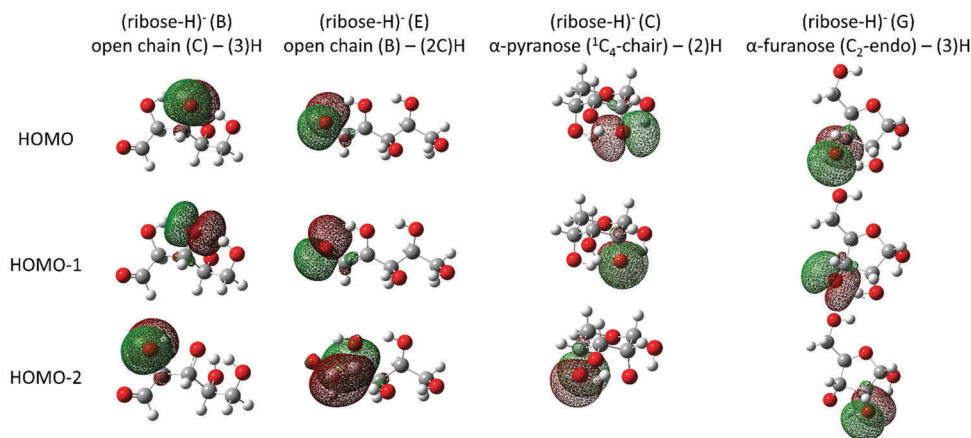

Fig. 8 Molecular orbitals of lower lying open chain, pyranose, and furanose structures of the (ribose-H)⁻ anion from an NBO analysis based on B3LYP/6-311++G(d,p) calculations. They are assigned to be present in the experiment based on the good agreement between experimental and theoretical VDEs.
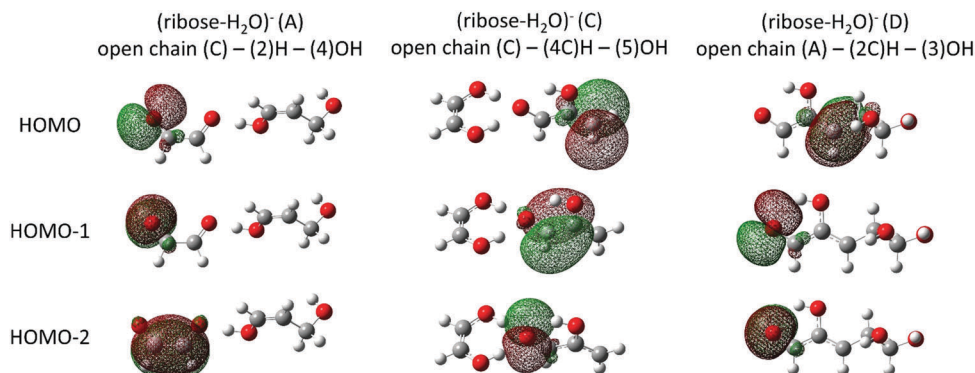
28958 | *Phys. Chem. Chem. Phys.,* 2017, **19**, 28950–28962

This journal is © the Owner Societies 2017

Fig. 9 Molecular orbitals (from an NBO analysis of B3LYP/6-311++G(d,p) calculations) for two positional isomers (C and D) of the (ribose-H_2O)$^-$ anion, as well as those of the most stable isomer (A). Isomers (C) and (D) are assigned to be present in the experiments, contributing to higher and lower electron binding energy components of the observed PES feature, respectively, based on the good agreement between experimental and theoretical VDEs.

Pyranose and furanose anionic conformations of ribose$^-$ and fructose$^-$ parent anions are much less stable than open chain ones. An NBO analysis shows that the additional electron distribution of cyclic anionic conformations for both saccharides is of a dipole bound character.

The calculated VDEs of open chain ribose$^-$ parent anions are 1.64, 1.73 and 1.51 eV, and those of open chain fructose$^-$ parent anions are 1.87, 1.57, and 1.46 eV. These VDEs evidence only slight differences. For both ribose$^-$ and fructose$^-$, such anionic open chain structures can arise from an open chain neutral molecule attaching an extra electron.

The calculated VDEs of cyclic ribose$^-$ parent anions are negative (from -0.03 to -0.25 eV), and those of cyclic fructose$^-$ parent anions are positive but near zero (from 0.04 to 0.24 eV). This result indicates that neutral ribose cyclic structures are unlikely to form negative cyclic ions, while the fructose cyclic conformations might be able to capture an excess electron. These EBE differences may provide a useful qualitative understanding for the possible mechanism associated with ring opening of cyclic structures for dissociative electron attachment experiments, for which a doorway mechanism has been proposed.[33] This doorway mechanism emphasizes that DEA to fructose can proceed by initial electron capture in a vibrational Feshbach resonance: this mechanism is supported by the dipole-bound state of the pyranose isomer of the fructose anion. According to this suggested process, following DEA an essentially simultaneous ring opening occurs, followed by transfer of the excess electron into the valence orbital of the open chain isomer.[33] Cyclic ribose may not be able to proceed with this ring opening mechanism because of its reduced ability to attach an electron. Such a ring opening process could occur in the present experiments for cyclic neutrals attaching an extra electron through the MALDI/ablation process.

Below, the absence of ribose$^-$ open chain parent anions from the TOFMS/PES results is considered in terms of anion dissociation or fragmentation processes. The ribose$^-$ open chain anion can rapidly fragment to (ribose-X)$^-$, X = H, H_2O, and consequently the parent anion is not present at high enough concentrations to be observed in the present experiments: the

situation for fructose$^-$ must be different, as the fructose$^-$ parent anion and all its fragment anions, –H, –OH, –H_2O, are still observed. The fructose open chain parent anion is apparently more stable to fragmentation than is the ribose open chain parent anion.

To explain the different stabilities of sugar open chain anions, the bond strengths and reaction barriers for specific fragmentations can also be analyzed. The average O–H bond strength of the most stable open chain anions for different sugars is similar. This is consistent with the fact that both (ribose-H)$^-$ and (fructose-H)$^-$, as presented as below, appear in the PES data. The average C–OH bond strength for the ribose$^-$ open chain parent anion is greater by ~ 70 kJ mol^{-1} than the corresponding fructose$^-$ open chain parent anion, as shown in Table S2 (ESI†). Thus, OH fragmentation from ribose$^-$ needs more energy than the similar fragmentations for fructose$^-$ based on the calculations. This suggestion is consistent with the absence of (ribose-OH)$^-$ and the presence of (fructose-OH)$^-$ in the experiments. Recall that generating (sugar-H_2O)$^-$ through direct loss of a H_2O molecule from parent anions/ neutrals is thermodynamically allowed. Relaxed potential energy surface scans of sugar open chain parent anions with regard to formation of a H_2O moiety directly as the first step for losing H_2O have also been calculated: these show a larger barrier for ribose$^-$ fragmentation than for fructose$^-$ fragmentation, as can be seen in Fig. S21 and S22 (ESI†). Therefore, loss of water from ribose is less energetically favorable than loss of water from fructose, even though both species are observed in the experiments. These bond strength and surface scan results suggest that the ribose$^-$ open chain parent anion is more stable to fragmentation (with –OH, –H_2O but not –H) than fructose$^-$ open chain parent anion is, and ribose$^-$ should be observed, because of the larger C–OH bond strength and larger barrier of H_2O unit formation for ribose$^-$ than fructose$^-$. Thus, the absence of ribose$^-$ anions from the ribose$^-$ PES data should not be understood by a step by step mechanism involving saccharide → saccharide$^-$ → (saccharide-X)$^-$ (X = H, OH, H_2O). We can suggest that from the experimental results, the ribose$^-$ open chain parent anion and the (ribose-OH)$^-$ anion are not as stable species as fructose$^-$

and (fructose-OH)⁻ during our MALDI/ablation process. Note too that the MALDI processes also involve electron capture and fragmentation reactions as can be imagined for early Earth electron capture and DEA mechanisms.

b. (Ribose-H)⁻ and (fructose-H)⁻. The PES of (ribsoe-H)⁻ and (fructose-H)⁻ displays similar broad major features at high EBE ($> \sim 3$ eV), but evident significant differences in a low EBE range ($< \sim 3$ eV). (Ribose-H)⁻ presents a higher intensity at the low EBE side of the feature than that of (fructose-H)⁻. High EBE components in these spectra are mostly contributed by isomers with loss of H from an O atom, but a few open chain isomers with loss of H from a C atom can also contribute PES features to the high EBE part of the spectrum. Low EBE components of both PES features can only be generated by open chain isomers losing a H atom from a C atom. Each detailed structural information is described below.

Note that both (ribose-H)⁻ and (fructose-H)⁻ are more likely to form during the laser ablation processes than from reaction chain mechanisms based on parent species.

Contributors to the high EBE PES features of (ribose-H)⁻ with loss of a H atom from an O atom can have open chain, pyranose, and/or furanose conformations, while (fructose-H)⁻ mostly evidences open chain and pyranose structures for this region of the PES feature. Furanose structures of (fructose-H)⁻ have a significantly higher relative energy (> 0.56 eV) with respect to the lowest energy isomer of (fructose-H)⁻. By comparing the O–H bond strength in furanose structures for ribose⁻ and fructose⁻, the strength of O–(1)H and O–(3)H bonds in ribose is 77 kJ mol⁻¹, while the strength of O–(2)H and O–(3)H bonds in fructose is above 112 kJ mol⁻¹, as shown in Table S3 (ESI†). Thus, ribofuranose⁻ has a relative higher propensity for loss of H than does fructofuranose⁻ in a MALDI/ablation process. If we consider that (sugar-H)⁻ comes from parent neutral by losing one proton, the proton loss position can indicate the acidic positions for hydroxyl groups. The lowest energy open chain structure loses (3)H and the lowest energy pyranose structure loses (2)H for both (ribose-H)⁻ and (fructose-H)⁻. This implies that the most acidic positions for hydroxyl groups in open chain or pyranose structures are the same for both sugar molecules.

The low EBE contributors to both PES features with loss of a H atom from a C atom are all open chain structures. For (ribose-H)⁻, the loss position is at (2C)H, which is adjacent to the carbonyl C. For (fructose-H)⁻, the loss positions can be (1C)H and (3C)H, also adjacent to the carbonyl C. These kinds of isomers for (ribose-H)⁻ have lower relative energy with respect to the lowest energy isomer of (ribose-H)⁻ than do the corresponding ones for (fructose-H)⁻. This can explain why (ribose-H)⁻ has a higher PES feature intensity in the low EBE components. Additionally, C–H ((2)C–H for ribose, (1)C–H and (3)C–H for fructose) bond strength of ribose⁻ is lower by ~ 40 kJ mol⁻¹ than that of fructose⁻. This comparison suggests that open chain ribose⁻ probably has a higher propensity for loss of H from C (which is adjacent to carbonyl) than open chain fructose⁻ does during the MALDI/ablation process.

c. (Ribose-H₂O)⁻ and (fructose-H₂O)⁻. (Ribose-H₂O)⁻ and (fructose-H₂O)⁻ show similar photoelectron spectral features (as can be seen in Fig. S23, ESI†) but with different assigned structures. They both present two types of positional isomers, but the two saccharides differ with regard to H₂O loss positions. (ribose-H₂O)⁻ evidences (4C)H/(5)OH and (2C)H/(3)OH isomers, while (fructose-H₂O)⁻ evidences (3)H/(6)OH and (5)H/(3)OH isomers. The two types of positional isomers of (ribose-H₂O)⁻ are both developed only from parent anion open chain structures, while those of (fructose-H₂O)⁻ are derived from parent anion open chain and furanose cyclic structures. This can indicate that ribofuranose has a lower decomposition probability through loss of water upon attaching an extra electron compared to fructofuranose.

(Ribose-H₂O)⁻ occurs through loss of a H from a C atom for both two positional isomers. This fragmentation is different from that for (fructose-H₂O)⁻, for which loss of a H atom from an O atom is a lower energy process. This further suggests the higher propensity for loss of H from C of open chain structures for the ribose⁻ anion than for the fructose⁻ anion, as can be supported by the bond strengths in anions shown in Table S2 (ESI†).

Both (ribose-H₂O)⁻ and (fructose-H₂O)⁻ possess isomers with C–C bond breaking, held together in isolation through hydrogen bonds. Both (ribose-H₂O)⁻ and (fructose-H₂O)⁻ can be generated either through the ablation process or through reaction pathways from parent anions or neutrals by direct loss of water.

VII. Conclusions

(1) Ribose related species

Anion photoelectron spectroscopy coupled with density functional theory based calculations are executed to characterize gas phase, isolated (ribose-H)⁻ and (ribose-H₂O)⁻ molecular anions produced using a MALDI method. Their vertical detachment energies are experimentally determined and the corresponding computed anionic structures are validated based on good agreement between experimental and theoretical vertical detachment energies. Both conformational and positional isomers are considered and assigned.

a. Ribose⁻. The ribose⁻ parent anion is not populated in a high enough concentration to be observed in the presented experiments. (ribose-H)⁻ and (ribose-H₂O)⁻ anions can be accessed as the characteristic fragmentation ions of the parent species. From the DFT based calculation results, open chain structures of the ribose⁻ parent anion are the lowest energy structures: cyclic (pyranose and furanose) geometries for the parent anion are of a much higher energy. An NBO analysis of the three types of structures (linear, furanose, and pyranose) suggests that open chain parent anions have a valence-bound added electron distribution, different from a diffuse dipole-bound electronic structure for cyclic geometries. Based on the fact that the parent ribose⁻ open chain anion should be generated in the MALDI/ablation process and that the isolated ribose⁻ open chain anion has a lower energy than the isolated ribose open chain neutral, the parent anion of ribose must be unstable with respect to the (ribose-X)⁻, X = H, H₂O species, and must therefore fragment in < 200 µs.

28960 | *Phys. Chem. Chem. Phys.*, 2017, **19**, 28950–28962

This journal is © the Owner Societies 2017

b. (Ribose-H)⁻. For the (ribose-H)⁻ anion, substrate dependent PES features evidence a broad electron binding energy range, suggesting that many coexisting isomers, both positional and conformational, exist in the experimental sample. The high EBE components are mostly contributed by isomers with loss of H from an O atom for both positional and conformational isomers of open chain, pyranose, and furanose structures. A few open chain isomers with loss of H from a C atom can also be identified from DFT calculations. The low EBE components of the PES feature for this anion can be assigned to the higher energy isomers. These high energy isomers of (ribose-H)⁻ are associated with structures undergoing loss of H from a (2)C atom. These anionic, isolated species derived from ribose are stable.

c. (Ribose-H₂O)⁻. (Ribose-H₂O)⁻ is mainly present in our experiments as two kinds of positional isomers, one with loss of (4C)H and (5)OH, the other with loss of (2C)H and (3)OH. Both are derived from open chain structures with loss of H from a C atom. Each positional isomer exhibits conformational differences. Positional isomers (4C)H/(5)OH incur C–C bond breaking and form intramolecular hydrogen bonds that stabilize and bind the resulting fragments.

From the thermodynamic point of view, the calculated enthalpy change (ΔH) for reactions from parent species (both anion and neutral) to (ribose-H)⁻ is positive and the reaction is therefore thermodynamically forbidden. On the other hand, negative ΔH values for the reaction from parent species to (ribose-H₂O)⁻, through loss of one water molecule directly, is thermodynamically allowed. Therefore, (ribose-H)⁻ is probably already present in the beam after the MALDI/ablation processes. (ribose-H₂O)⁻ can be generated either from the MALDI/ablation processes itself or from both reaction pathways from the parent anion or neutral through loss of one H₂O molecule directly. This conclusion is consistent with the experimental observation that the photoelectron spectrum of (ribose-H)⁻ is substrate dependent, and that similar PES features of (ribose-H₂O)⁻ are obtained with different substrates. Determination of fixed positions for loss of H₂O that are different from random loss of H from all C and O positions also suggests direct, spontaneous processes for loss of water.

(2) Comparison between the ribose and fructose results

By conducting comparisons between ribose and fructose PES and calculation results, more significant differences are found between respective furanose and between respective open chain structures, than between pyranose structures. Ribose⁻ open chain structures are more likely to lose hydrogen from a C atom than are fructose⁻ open chain structures. Ribofuranose⁻ has a relatively higher propensity for loss of H than does fructofuranose⁻ in our MALDI/ablation process. Ribofuranose has a smaller decomposition probability through loss of water upon attaching an extra electron than does fructofuranose. Ribofuranose is apparently more stable than fructofuranose. Based on the electronic and reactivity properties, and on stability toward radiation/electron capture damage, this could be one reason that ribose has been favored for the DNA/RNA backbone rather than fructose, since the sugar moiety presents a furanose cyclic structure for

DNA/RNA backbone supports. Of course, steric and spacing issues cannot be ignored as other potential reasons for the biological selection of ribose species over other saccharides for the DNA/RNA backbone support. Moreover, the DNA/RNA backbone includes a sugar moiety and a phosphate moiety, in addition to central aromatic nitrogenous bases. Further studies dealing with these substituted sugar moieties will be performed to understand the detailed unique choice of ribose/deoxyribose over other possible saccharide and substituted saccharide couples. The factors that contribute to the evolutionary choice of ribose over other saccharides as the backbone support for genetic related molecules have been associated with size and steric effects, which have been presented and reviewed[21,34,35] by Eschenmoser and others.

Conflicts of interest

There are no conflicts of interest to declare.

Acknowledgements

References

1 M. Rudrum and D. F. Shaw, *J. Chem. Soc.*, 1965, 52, DOI: 10.1039/jr9650000052.

2 E. Breitmaier and U. Hollstein, *Org. Magn. Reson.*, 1976, **8**, 573.

3 S. J. Angyal, *Angew. Chem., Int. Ed. Engl.*, 1969, **8**, 157.

4 M. J. King-Morris and A. S. Serianni, *J. Am. Chem. Soc.*, 1987, **109**, 3501.

5 D. Šišak, L. B. McCusker, G. Zandomeneghi, B. H. Meier, D. Bläser, R. Boese, W. B. Schweizer, R. Gilmour and J. D. Dunitz, *Angew. Chem., Int. Ed.*, 2010, **49**, 4503.

6 E. J. Cocinero, A. Lesarri, P. Écija, F. J. Basterretxea, J.-U. Grabow, J. A. Fernández and F. Castaño, *Angew. Chem., Int. Ed.*, 2012, **51**, 3119.

7 L. M. Azofra, M. M. Quesada-Moreno, I. Alkorta, J. R. Aviles-Moreno, J. J. Lopez-Gonzalez and J. Elguero, *New J. Chem.*, 2014, **38**, 529.

8 M. Szczepaniak and J. Moc, *Carbohydr. Res.*, 2014, **384**, 20.

9 I. Bald, H. D. Flosadóttir, J. Kopyra, E. Illenberger and O. Ingólfsson, *Int. J. Mass Spectrom.*, 2009, **280**, 190.

10 B. Boudaïffa, P. Cloutier, D. Hunting, M. A. Huels and L. Sanche, *Science*, 2000, **287**, 1658.

11 F. Martin, P. D. Burrow, Z. Cai, P. Cloutier, D. Hunting and L. Sanche, *Phys. Rev. Lett.*, 2004, **93**, 068101.

12 L. Sanche, *Eur. Phys. J. D*, 2005, **35**, 367.

This journal is © the Owner Societies 2017

Phys. Chem. Chem. Phys., 2017, **19**, 28950–28962 | 28961

13 S. Ptasińska, S. Denifl, S. Gohlke, P. Scheier, E. Illenberger and T. D. Märk, *Angew. Chem., Int. Ed.*, 2006, **45**, 1893.

14 I. Bald, J. Kopyra and E. Illenberger, *Angew. Chem., Int. Ed.*, 2006, **45**, 4851.

15 I. Baccarelli, F. A. Gianturco, A. Grandi, N. Sanna, R. R. Lucchese, I. Bald, J. Kopyra and E. Illenberger, *J. Am. Chem. Soc.*, 2007, **129**, 6269.

16 T. Fujita, M. Kondo and T. Takayanagi, *Comput. Theor. Chem.*, 2016, **1075**, 70.

17 M. W. Powner, J. D. Sutherland and J. W. Szostak, *Synlett*, 2011, 1956.

18 G. Banfalvi, *DNA Cell Biol.*, 2006, **25**, 189.

19 R. Bielski and M. Tencer, *Origins Life Evol. Biospheres*, 2007, **37**, 167.

20 G. Springsteen and G. F. Joyce, *J. Am. Chem. Soc.*, 2004, **126**, 9578.

21 A. Eschenmoser, *Science*, 1999, **284**, 2118.

22 Z. Zeng and E. R. Bernstein, *Phys. Chem. Chem. Phys.*, 2017, **19**, 23325.

23 H.-S. Im and E. R. Bernstein, *J. Chem. Phys.*, 2000, **113**, 7911.

24 S. Yin and E. R. Bernstein, *J. Chem. Phys.*, 2016, **145**, 154302.

25 B. Yuan, Z. Yu and E. R. Bernstein, *J. Chem. Phys.*, 2015, **142**, 124315.

26 A. D. Becke, *J. Chem. Phys.*, 1993, **98**, 5648.

27 C. Lee, W. Yang and R. G. Parr, *Phys. Rev. B: Condens. Matter Mater. Phys.*, 1988, **37**, 785.

28 A. D. Becke, *Phys. Rev. A: At., Mol., Opt. Phys.*, 1988, **38**, 3098.

29 M. J. Frisch, G. W. Trucks, H. B. Schlegel, G. E. Scuseria, M. A. Robb, J. R. Cheeseman, G. Scalmani, V. Barone, B. Mennucci, G. A. Petersson, H. Nakatsuji, M. Caricato, X. Li, H. P. Hratchian, A. F. Izmaylov, J. Bloino, G. Zheng, J. L. Sonnenberg, M. Hada, M. Ehara, K. Toyota, R. Fukuda, J. Hasegawa, M. Ishida, T. Nakajima, Y. Honda, O. Kitao, H. Nakai, T. Vreven, J. A. M. Jr., J. E. Peralta, F. Ogliaro, M. Bearpark, J. J. Heyd, E. Brothers, K. N. Kudin, V. N. Staroverov, R. Kobayashi, J. Normand, K. Raghavachari, A. Rendell, J. C. Burant, S. S. Iyengar, J. Tomasi, M. Cossi, N. Rega, J. M. Millam, M. Klene, J. E. Knox, J. B. Cross, V. Bakken, C. Adamo, J. Jaramillo, R. Gomperts, R. E. Stratmann, O. Yazyev, A. J. Austin, R. Cammi, C. Pomelli, J. W. Ochterski, R. L. Martin, K. Morokuma, V. G. Zakrzewski, G. A. Voth, P. Salvador, J. J. Dannenberg, S. Dapprich, A. D. Daniels, O. Farkas, J. B. Foresman, J. V. Ortiz, J. Cioslowski and D. J. Fox, *Gaussian 09, Revision A.02*, Gaussian, Inc., Wallingford CT, 2009.

30 Y. Zhao and D. G. Truhlar, *Theor. Chem. Acc.*, 2008, **120**, 215.

31 Y. Zhao and D. G. Truhlar, *Acc. Chem. Res.*, 2008, **41**, 157.

32 J.-D. Chai and M. Head-Gordon, *Phys. Chem. Chem. Phys.*, 2008, **10**, 6615.

33 T. Sommerfeld, *J. Chem. Phys.*, 2007, **126**, 124301.

34 A. Eschenmoser and M. Dobler, *Helv. Chim. Acta*, 1992, **75**, 218.

35 G. Otting, M. Billeter, K. Wüthrich, H.-J. Roth, C. Leumann and A. Eschenmoser, *Helv. Chim. Acta*, 1993, **76**, 2701.